

Unexpected highly reversible topotactic CO₂ sorption/desorption capacity for potassium dititanate

Qianwen Zheng¹, Liang Huang¹, Yu Zhang¹, Junya Wang¹, Chen-Zi Zhao², Qiang
Zhang², Weijie Zheng³, Dapeng Cao³, Dermot O'Hare⁴, Qiang Wang^{1,*}

¹College of Environmental Science and Engineering, Beijing Forestry University, 35
Tsinghua East Road, Haidian District, Beijing 100083, P. R. China

²Department of Chemical Engineering, Tsinghua University, 1 Tsinghua Road, Haidian
District, Beijing 100084, P. R. China

³Division of Molecular and Materials Simulation, State Key Laboratory of
Organic-Inorganic Composites, Beijing University of Chemical Technology, Beijing
100029, P. R. China

⁴Chemistry Research Laboratory, Department of Chemistry, University of Oxford,
Mansfield Road, Oxford OX1 3TA, United Kingdom

*Corresponding author:

Professor Qiang Wang, College of Environmental Science and Engineering, Beijing
Forestry University, 35 Qinghua East Road, Haidian District, Beijing 100083, P. R.
China

Tel.: 86-13699130626

E-mail: qiang.wang.ox@gmail.com; qiangwang@bjfu.edu.cn

Abstract

Potassium dititanate ($\text{K}_2\text{Ti}_2\text{O}_5$) was revealed to possess an unexpected highly reversible CO_2 sorption/desorption capacity at *ca.* 750 °C, which is promising as high-temperature CO_2 adsorbent for sorption enhanced hydrogen production (SEHP) processes. In contrast to many other adsorbents which sinter severely during cycles at high-temperatures, the CO_2 sorption/desorption cycles over $\text{K}_2\text{Ti}_2\text{O}_5$ exhibited a contrast particle size “break-down” process. The large $\text{K}_2\text{Ti}_2\text{O}_5$ particles gradually break-down into $\text{K}_2\text{Ti}_2\text{O}_5$ nanofibers after 20 cycles, leading to a very stable CO_2 sorption/desorption performance with very rapid kinetics. A reversible CO_2 capture capacity as high as 7.2 wt% was achieved at 750 °C. What’s more, only 6 min is required for complete CO_2 desorption at 750 °C, indicating this adsorbent can be practically run with a simply pressure swing sorption scheme. Surprisingly, an interesting structure switching phenomenon between $\text{K}_2\text{Ti}_2\text{O}_5$ and $\text{K}_2\text{Ti}_4\text{O}_9$ caused by CO_2 sorption and desorption was revealed. A detailed mechanism was proposed based on XRD, FTIR, SEM, HR-TEM, and SAED analyses, and was further verified by density functional theory calculation. Considering its relatively high CO_2 capture capacity, superior cycling stability, and excellent regeneration ability, we believe $\text{K}_2\text{Ti}_2\text{O}_5$ offers significant potential as a practical novel high-temperature CO_2 adsorbent.

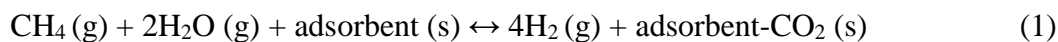
Keywords: $\text{K}_2\text{Ti}_2\text{O}_5$; reversible structure switching; CO_2 sorption/desorption mechanism; sorption enhanced hydrogen production; global warming

1. Introduction

There is a general agreement that the CO₂ emission resulted from the burning of fossil fuels is one of the major reasons for the climate change.¹⁻³ It is expected that the energy demand will increase further by 53% by 2030, and fossil fuels will still be the dominant source in the next few decades.⁴ In order to prevent these disastrous effects, there is now need for a continuing and significant global effort to develop new technologies/processes for CO₂ capture, storage (sequestration) and utilization (CSU).⁵⁻⁹ CSU is believed to be able to significantly reduce the amount of anthropogenic energy-related CO₂ emissions, and contribute to global climate change mitigation.¹⁰ Among all the CO₂ capture technologies,¹¹ great attention has been devoted to pre-combustion CO₂ capture, particularly on the sorption enhanced steam reforming (SESR) processes.¹²⁻¹⁴

Currently, more than 50 million tons of H₂ is produced annually, of which the majority is provided by a conventional steam methane reforming route because of the maturity of the technology and its favorable economics.¹⁵ However, in order to further increase the H₂ production efficiency and lower the CO₂ emission, the SESR process has been developed recently, which is believed to be more economical, energy efficient, and environmentally friendly, as shown in reaction (1).^{12, 13} Since this reaction is equilibrium limited, it is impossible to achieve a complete conversion of CH₄ or CO in a single reactor under normal reaction conditions. However, if the CO₂ byproduct can be removed from the gas phase (*e.g.* by sorption on a solid CO₂ adsorbent), the normal equilibrium limits are removed and a complete conversion can be approached. In addition, it process produces pure CO₂, which may be compressed and transported for further storage and

utilization.^{15, 16} For the above mentioned SESR process, designing proper high-temperature CO₂ adsorbents is crucial for its practical implementation.



Up to date, there are mainly three types of high-temperature CO₂ adsorbents have been reported for SESR, which are CaO,^{5, 13} Li₂ZrO₃ (alkali zirconates),¹⁷⁻¹⁹ and Li₄SiO₄ (alkali silicates).²⁰⁻²² Although great progresses have been achieved with the above three types of adsorbents, each of them still has their own drawbacks, such as thermal sintering, low kinetics, etc. In this contribution, we are reporting the fourth example, K₂Ti₂O₅ (alkali dititanates) as a novel type of high-temperature CO₂ adsorbent. The present work reports the first study on the high-temperature CO₂ capture performance of potassium titanates (K₂Ti₂O₅, K₂Ti₄O₉, and K₂Ti₆O₁₃). Their CO₂ capture capacities were evaluated using thermogravimetric analysis (TGA) at 200–800 °C. The CO₂ sorption and desorption mechanism over the best adsorbent K₂Ti₂O₅ was investigated using XRD, FTIR, SEM, HR-TEM, SAED, and DFT calculation. The kinetics and cycling stability were also evaluated, and all results demonstrated that K₂Ti₂O₅ is a promising high-temperature CO₂ adsorbent for application in SEHP processes.

2. Experimental

2.1 Synthesis of potassium titanates

Three types of potassium titanates, K₂Ti₂O₅, K₂Ti₄O₉, and K₂Ti₆O₁₃ were synthesized by solid state reaction method. Potassium carbonate (Sinopharm Chemical Reagent Co., Ltd.) and titanium dioxide (Sigma-Aldrich (Wuxi) Life Science & Technology Co., Ltd.) were mixed together, and ground to fine powder in agate mortar for a certain time. The molar

ratio of $\text{K}_2\text{CO}_3\text{:TiO}_2 = 1\text{:}2, 1\text{:}4, 1\text{:}6$ was chosen for $\text{K}_2\text{Ti}_2\text{O}_5$, $\text{K}_2\text{Ti}_4\text{O}_9$, and $\text{K}_2\text{Ti}_6\text{O}_{13}$, respectively. After that, they were calcined at 850, 970, and 1080 °C for 10.0 h in air to obtain $\text{K}_2\text{Ti}_2\text{O}_5$, $\text{K}_2\text{Ti}_4\text{O}_9$, and $\text{K}_2\text{Ti}_6\text{O}_{13}$, respectively, followed by cooling and crushing to fine powders.

2.2 Characterization of $\text{K}_2\text{Ti}_2\text{O}_5$

Powder X-ray diffraction (XRD) analyses were conducted in a Shimadzu XRD-7000 instrument in reflection mode with Cu K α radiation and a power of 40 kV \times 40 mA. Diffraction patterns were recorded within the range of $2\theta = 5\text{--}80^\circ$ with a step size of 0.02° . The morphology of synthesized potassium titanates was observed using scanning electron microscopy (SEM, Hitachi S-3400N II). Before observation, the dried samples were sputtered and coated with gold for ~ 120 s under an Ar atmosphere. High resolution transmission electron microscopy (HR-TEM) and selected area electron diffraction patterns (SAED) were performed on JEM-2010F (JEOL, Japan) microscope with an accelerating voltage of 200 kV. Attenuated total reflectance-Fourier transform infrared spectroscopy (ATR-FTIR) spectrum of samples was measured using a Bruker Vertex 70 spectrophotometer. The thermal stability of samples was determined using a Q50 TGA (TA Instruments) in N_2 with a flow rate of 40 mL/min. Typically, about 40 mg of sample was used for each run. The samples were placed in a Pt sample pan and heated from room temperature to 800 °C with a ramping rate of 10 °C/min.

2.3 CO_2 capture evaluation

Sorption of CO_2 on $\text{K}_2\text{Ti}_2\text{O}_5$, $\text{K}_2\text{Ti}_4\text{O}_9$, and $\text{K}_2\text{Ti}_6\text{O}_{13}$ was determined using a thermal gravimetric method on a Q50 TGA analyzer. All samples were pre-calcined at 750 °C for 1.0 h under a flow of 100% N_2 to remove the pre-absorbed species. CO_2 sorption

experiments were carried out at certain temperatures for 2.0 h (*e.g.* 200, 300, 350, 700, 750, and 800 °C, respectively), and 1.0 atm with a constant flow of CO₂ (40 mL/min). Temperature programmed desorption (TPD) of CO₂ was carried out with a fixed bed reactor equipped with a tube furnace. The sample was heated up to 800 °C with a heating rate of 5 °C/min. The desorbed CO₂ was monitored using an on-line quadrupole mass spectrometer (Hidden, UK).

Cycling tests were also performed with a TGA analyzer. Approximately 40 mg of K₂Ti₂O₅ was loaded in a Pt pan. Before cycling test, the sample was heated up to 750 °C at a ramping rate of 10 °C/min under pure N₂. In a typical run, the sorption process was tested at 750 °C in CO₂ for 1.0 h. After sorption, the gas was switched to pure N₂ for desorption at 750 °C for 10 min. The CO₂ sorption and desorption cycles were repeated for 20 times.

2.4 Calculation details

Theoretical calculations for K₂Ti₂O₅ and K₂Ti₄O₉ were based on density functional theory (DFT) implemented in the Vienna Ab initio Simulation Package (VASP).^{23, 24} The projector augmented wave (PAW) method^{25, 26} was used in our calculation and the generalized gradient approximation (GGA) of the Perdew–Burke–Ernzerhof (PBE)²⁷ form was adopted to describe the exchange and correlation potentials. An energy cutoff of 500 eV were employed for plane-wave basis throughout this work. All energy calculations were done with a Monkhorst–Pack k-point mesh of $7 \times 7 \times 5$ with energy converged to 1.0×10^{-4} eV/atom.

3. Results and discussion

3.1 Synthesis and characterization of potassium titanates

Potassium titanates were synthesized using a simple solid state method, which is suitable for large scale preparation. In order to obtain well crystallized $\text{K}_2\text{Ti}_2\text{O}_5$, $\text{K}_2\text{Ti}_4\text{O}_9$, and $\text{K}_2\text{Ti}_6\text{O}_{13}$, the mixture of TiO_2 and K_2CO_3 was calcined at 850, 970, and 1080 °C in air for 10.0 h, respectively. Figure 1(a) shows the XRD patterns of the obtained potassium titanates samples, they all exhibit a good consistency with the reported XRD patterns respectively (PDF51–1890, PDF32–0861, and PDF40–0403). $\text{K}_2\text{Ti}_2\text{O}_5$ possesses unit cell dimensions $a = 11.374 \text{ \AA}$, $b = 3.799 \text{ \AA}$, $c = 6.616 \text{ \AA}$, $\beta = 100.1^\circ$, the structure satisfies the space group of C2/m. On prolonged sintering of $\text{K}_2\text{Ti}_2\text{O}_5$, the (001) Bragg reflection is significantly stronger than the (111) reflection due to texture (preferred orientation) effects. $\text{K}_2\text{Ti}_4\text{O}_9$ possesses unit cell dimensions $a = 18.250 \text{ \AA}$, $b = 3.791 \text{ \AA}$, $c = 12.010 \text{ \AA}$, and $\beta = 106.4^\circ$, while $\text{K}_2\text{Ti}_6\text{O}_{13}$ possesses a monoclinic crystal structure with $a = 15.593 \text{ \AA}$, $b = 3.796 \text{ \AA}$, $c = 9.108 \text{ \AA}$, $\beta = 99.78^\circ$, with a space group of C2/m. No impurity reflections were observed in these patterns, suggesting that the as-synthesized $\text{K}_2\text{Ti}_2\text{O}_5$, $\text{K}_2\text{Ti}_4\text{O}_9$, and $\text{K}_2\text{Ti}_6\text{O}_{13}$ are all phase pure. The inset of Figure 1(a) shows the schematic structure of $\text{K}_2\text{Ti}_2\text{O}_5$. The titanium atoms are each co-ordinated to five oxygens grouped as a slightly distorted trigonal bipyramid, and this double unit forms an endless string elongated along the y direction. The layers are held together by the potassium atoms. According to theoretical calculation and model simulation for $\text{K}_2\text{Ti}_2\text{O}_5$, the bond distance of the five Ti–O bonds was obtained, which was 1.58, 1.91, 1.98, 1.99, and 1.98 Å, respectively.

The morphology of the synthesized potassium titanates were examined by SEM analysis (Figure 1(b–d)). Figure 1(b) indicates that irregular flat plate-like crystals of

$\text{K}_2\text{Ti}_2\text{O}_5$ with a particle size ranging from several micrometers to several-tenth micrometers were formed. $\text{K}_2\text{Ti}_4\text{O}_9$ formed whisker-type particles with an average width of 200 nm and a length of 5 μm , and $\text{K}_2\text{Ti}_6\text{O}_{13}$ exhibited rod-type particle morphology with an average width of 5 μm and a length of 10 μm . The SEM data show that the average particle size for both $\text{K}_2\text{Ti}_4\text{O}_9$ and $\text{K}_2\text{Ti}_6\text{O}_{13}$ are much smaller than $\text{K}_2\text{Ti}_2\text{O}_5$.

3.2 Decomposition and carbonation of potassium titanates

The decomposition and carbonation properties of the three potassium titanates were evaluated using TGA analysis in the presence of either N_2 or CO_2 (Figure 2(a–c)). The TGA profiles of decomposition processes suggested that all three potassium titanates possessed very high thermal stability, with very little weight loss in the temperature range from 50 to 800 °C. For instance, the final weight loss for $\text{K}_2\text{Ti}_2\text{O}_5$, $\text{K}_2\text{Ti}_4\text{O}_9$, and $\text{K}_2\text{Ti}_6\text{O}_{13}$ was only 3.0, 0.4, and 0.1 wt%, respectively. This is to be expected since all these samples were synthesized at temperatures higher than 850 °C. For $\text{K}_2\text{Ti}_2\text{O}_5$, the major weight loss occurred in the temperature range of 50–200 °C, which is attributed to the desorption of surface water. During the carbonation processes, the trends in weight change for $\text{K}_2\text{Ti}_4\text{O}_9$ and $\text{K}_2\text{Ti}_6\text{O}_{13}$ were similar to those occurred during the decomposition processes. Both $\text{K}_2\text{Ti}_4\text{O}_9$ and $\text{K}_2\text{Ti}_6\text{O}_{13}$ resulted in a weight loss, which was 0.5 and 0.2 wt%, respectively. While for $\text{K}_2\text{Ti}_2\text{O}_5$, it also displayed a weight loss in the temperature range of 50–200 °C, and its weight then started to increase above 200 °C due to the sorption of CO_2 , and finally reached about 100.5%. These results demonstrated that the CO_2 sorption capacities of both $\text{K}_2\text{Ti}_4\text{O}_9$ and $\text{K}_2\text{Ti}_6\text{O}_{13}$ were very poor, and nearly no CO_2 can be captured on either of these two potassium titanates. These data also

suggested that only $\text{K}_2\text{Ti}_2\text{O}_5$ has the capability to capture CO_2 , particularly at the temperature range 600–800 °C. This is the first demonstration of CO_2 capture for $\text{K}_2\text{Ti}_2\text{O}_5$. Furthermore, among the different potassium titanates, the CO_2 capture capability is unique to $\text{K}_2\text{Ti}_2\text{O}_5$.

3.3 CO_2 capture performance of $\text{K}_2\text{Ti}_2\text{O}_5$

The carbonation experiments had demonstrated that $\text{K}_2\text{Ti}_2\text{O}_5$ had great potential as a high-temperature CO_2 adsorbent. To illustrate the potential of $\text{K}_2\text{Ti}_2\text{O}_5$ for SEHP processes, its isothermal CO_2 capture capacity was evaluated. Figure 2(d) shows the effect of sorption temperature on the CO_2 capture capacity of $\text{K}_2\text{Ti}_2\text{O}_5$. The highest CO_2 uptake was achieved at around 750 °C. Before 750 °C, the sorption capacity increased with the increase in temperature, with a value of 0.62, 1.58, and 1.67 wt% at 200, 300, and 350 °C, respectively. When the temperature was high, the CO_2 sorption capacity was notably improved, and reached 5.0 and 6.4 wt% at 700 and 750 °C, respectively. However, upon further increase in the sorption temperature to 800 °C, the CO_2 sorption capacity started to decrease (4.9 wt%). This is because the sorbed CO_2 starts to desorb when the temperature was too high. These data indicated that the optimal CO_2 sorption temperature for $\text{K}_2\text{Ti}_2\text{O}_5$ is 750 °C. TGA data in Figure S1 demonstrated that a rapid release of sorbed CO_2 can be achieved within 6.0 min after sorbed pure CO_2 at 750 °C for 300.0 min. The excellent regeneration ability is also an important advantage for $\text{K}_2\text{Ti}_2\text{O}_5$. We have also compared the isothermal CO_2 capture capacity of $\text{K}_2\text{Ti}_2\text{O}_5$, $\text{K}_2\text{Ti}_4\text{O}_9$, and $\text{K}_2\text{Ti}_6\text{O}_{13}$ at 750 °C (Figure 2(e)). It shows that only $\text{K}_2\text{Ti}_2\text{O}_5$ exhibits a rapid weight increase due to CO_2 sorption. The uptake exceeded 6.4 wt% after capturing CO_2 for 2.0 h.

However, with the same temperature (750 °C) and time (2.0 h), neither $\text{K}_2\text{Ti}_4\text{O}_9$ nor $\text{K}_2\text{Ti}_6\text{O}_{13}$ exhibited any CO_2 capture. These data demonstrate that $\text{K}_2\text{Ti}_2\text{O}_5$ has an excellent CO_2 capture capacity and good potential for SEHP applications.

3.4 CO_2 sorption/desorption mechanism over $\text{K}_2\text{Ti}_2\text{O}_5$

In order to understand the CO_2 sorption and desorption mechanism, $\text{K}_2\text{Ti}_2\text{O}_5$ was exposed to CO_2 at 750 °C for a given time (1.0, 5.0, and 10.0 h), and the structural and morphological changes as a function of sorption time were monitored using XRD, FTIR, and SEM analyses. The XRD data in Figure 3 clearly shows that, by the sorption of CO_2 , the structure of $\text{K}_2\text{Ti}_2\text{O}_5$ gradually transformed into $\text{K}_2\text{Ti}_4\text{O}_9$ and K_2CO_3 . With the increase of CO_2 sorption time, the characteristic Bragg reflections of $\text{K}_2\text{Ti}_2\text{O}_5$ disappear and concomitantly, the characteristic Bragg reflections of $\text{K}_2\text{Ti}_4\text{O}_9$ and K_2CO_3 grow in intensity. After CO_2 sorption for 10.0 h, the dominant Bragg reflections at $2\theta = 10.1^\circ$ is much weaker and broader than that from a sample of $\text{K}_2\text{Ti}_4\text{O}_9$ synthesized by the traditional solid state route, indicating that the particle size of $\text{K}_2\text{Ti}_4\text{O}_9$ formed by CO_2 sorption is very small. After annealing the sample in pure N_2 at 750 °C, all the characteristic Bragg reflections of $\text{K}_2\text{Ti}_4\text{O}_9$ and K_2CO_3 disappeared and the structure transformed back to $\text{K}_2\text{Ti}_2\text{O}_5$, indicating that the structure transformation is reversible.

The process was also monitored by infrared spectroscopy, as shown in Figure 4. After CO_2 sorption on $\text{K}_2\text{Ti}_2\text{O}_5$ at 750 °C for 1.0, 5.0, and 10.0 h, the characteristic peaks of $\text{K}_2\text{Ti}_4\text{O}_9$ were observed at 517, 771, and 939 cm^{-1} . The peaks at 517 cm^{-1} and 939 cm^{-1} were ascribed to the vibration of $\text{Ti}=\text{O}$ bond.²⁸ The peak at 771 cm^{-1} was due to the bridging $\mu^2\text{-O-Ti}$ vibration. Upon capturing CO_2 , the vibration of CO_3^{2-} was observed at

ca. 673 cm⁻¹.²⁹ Meanwhile, it is clear that the peaks centred at 1440 and 1050 cm⁻¹ increased in intensity after capturing CO₂.³⁰ The 1430–1460 cm⁻¹ peaks are probably caused by the presence of K₂CO₃.^{31, 32} After regenerating the CO₂-sorbed K₂Ti₂O₅ sample with pure N₂, most characteristic peaks of K₂Ti₄O₉ disappeared and the similar FTIR pattern as that of fresh K₂Ti₂O₅ was obtained. And due to the existence of peaks at 673 and 771 cm⁻¹, the regeneration process might not be completely. These data further suggested that the CO₂ sorption and desorption over K₂Ti₂O₅ can be explained by a reversible structure switching mechanism between K₂Ti₂O₅ and K₂Ti₄O₉, accompanied by the formation of K₂CO₃.

The proposed reversible structural transformation during CO₂ sorption and desorption was also investigated using SEM (Figure 5). Fresh K₂Ti₂O₅ showed flat, plate-like particles with relatively clean and smooth surfaces (Figure 5(a)). However, after adsorbing CO₂ for 1.0 h, many cracks were found on the surface, indicating that the large particles began to be disintegrated into smaller pieces. With the increase in CO₂ sorption time, the particles became increasingly rough. After 10.0 h sorption, its structure was completely destroyed and collapsed into nanofibers corresponding to the formation of K₂Ti₄O₉ (Figure 5(b–d)). The formation of nano-sized crystallites of K₂Ti₄O₉ is consistent with the XRD analysis. In order to prove that the morphology change is due to the sorption of CO₂, K₂Ti₂O₅ was tested under the same conditions (750 °C for 10.0 h) in N₂. Figure S2 indicates that the morphology of K₂Ti₂O₅ treated in N₂, like fresh K₂Ti₂O₅, showed big particles with an average size of 5–10 μm.

HRTEM and SAED were employed to further verify the K₂Ti₂O₅–K₂Ti₄O₉ structure switching phenomenon during CO₂ sorption/desorption over K₂Ti₂O₅ (JCPDS, PDF51–

1890) (Figure 6). Figure 6(a) and (b) show the TEM and SAED images of fresh $\text{K}_2\text{Ti}_2\text{O}_5$ before CO_2 sorption, in which the diffraction spots for the (020), $(2\bar{2}2)$ and $(20\bar{2})$ planes in $\text{K}_2\text{Ti}_2\text{O}_5$ were observed consistent with their interplanar spacing, with the [101] direction as the zone axis. This data confirmed the formation of the single crystals of $\text{K}_2\text{Ti}_2\text{O}_5$ before CO_2 sorption. Figure 6(c) and (d) show the TEM and SAED images of freshly synthesized $\text{K}_2\text{Ti}_4\text{O}_9$. The diffraction spots for the (020), (211), (402), and (422) planes were clearly detected in the SAED pattern with the $[10\bar{2}]$ direction as the zone axis. Figure 6(e) and (f) show the TEM and SAED analyses of the $\text{K}_2\text{Ti}_2\text{O}_5$ sample after adsorbing CO_2 for 10.0 h. According to our previous XRD and FTIR analyses, the $\text{K}_2\text{Ti}_2\text{O}_5$ crystals transform into $\text{K}_2\text{Ti}_4\text{O}_9$ crystals due to the abstraction of K ions by CO_2 . Thus, the CO_2 sorbed $\text{K}_2\text{Ti}_2\text{O}_5$ sample is expected to exhibit a diffraction pattern of $\text{K}_2\text{Ti}_4\text{O}_9$. The SAED diffraction pattern in Figure 6(f) indeed confirmed our proposed mechanism, in which the diffraction spots of the (020) and $(4\bar{0}4)$ planes of $\text{K}_2\text{Ti}_4\text{O}_9$ were observed, with the $[10\bar{2}]$ direction as the crystal zone axis.

In order to thoroughly demonstrate the CO_2 sorption on $\text{K}_2\text{Ti}_2\text{O}_5$ is reversible, in another word, the formed $\text{K}_2\text{Ti}_4\text{O}_9$ and K_2CO_3 could transform back to $\text{K}_2\text{Ti}_2\text{O}_5$, a new experiment was designed. We deliberately mixed a proper ratio (1:1) of $\text{K}_2\text{Ti}_4\text{O}_9$ and K_2CO_3 and calcined the mixture at 750 °C for different hours. The inverse process was analyzed using XRD (Figure S3), which clearly showed that the transformation between $\text{K}_2\text{Ti}_4\text{O}_9$ and $\text{K}_2\text{Ti}_2\text{O}_5$ occurs quickly, even within 1.0 h. For the mixture of $\text{K}_2\text{Ti}_4\text{O}_9$ and K_2CO_3 , the characteristic reflections of both were clearly observed. With the increase in calcination time, the peaks for $\text{K}_2\text{Ti}_4\text{O}_9$ and K_2CO_3 (JCPDS, PDF16–0820) disappeared or significantly weakened, and concomitantly the characteristic reflections of $\text{K}_2\text{Ti}_2\text{O}_5$

appeared and grew in intensity. Therefore, this experiment further verified the reversible structure switching mechanism between $\text{K}_2\text{Ti}_2\text{O}_5$ and $\text{K}_2\text{Ti}_4\text{O}_9$, accompanied by the formation of K_2CO_3 .

According to the above discussions, a deeper understanding of the CO_2 sorption/desorption mechanism over $\text{K}_2\text{Ti}_2\text{O}_5$ was proposed as Figure 7. $\text{K}_2\text{Ti}_2\text{O}_5$ exhibits a unique layered structure in which co-ordinate Ti atoms form a sheet of edge-sharing distorted bipyramids, the two-dimensional sheets or layers have a composition $(\text{Ti}_2\text{O}_5)^{2-}$. The layers are sandwiched by the potassium cations, which afford a curious unsymmetrical environment of eight oxygens, bearing only a superficial resemblance to the cubic site of the perovskite structure.³³ Because the molecular size of CO_2 (~ 0.33 nm) is much smaller than the distance between adjacent $(\text{Ti}_2\text{O}_5)^{2-}$ sheets (0.65 nm), it is possible for CO_2 to penetrate into the inter-layers and react with K^+ located inside the layers at a certain temperature (600–800 °C). The shortage of potassium led $\text{K}_2\text{Ti}_2\text{O}_5$ to be transformed into $\text{K}_2\text{Ti}_4\text{O}_9$ with a low K/Ti value. The crystal structure of $\text{K}_2\text{Ti}_4\text{O}_9$ consists of many structural units connected through aligned TiO_6 octahedra. The four TiO_6 octahedra form a line of framework by edge-sharing and further constructs staggered sheets with a zigzag string by corner-sharing with the interlayer space of 0.88 nm.³⁴ Because K_2CO_3 possesses unit cell dimensions $a = 5.640$ Å, $b = 9.831$ Å, and $c = 6.874$ Å (PDF87–0730), the formation of K_2CO_3 inside the layers finally led the large particles to be disintegrated into nano-fibers. By removing the sorbed CO_2 , the released K reacts with $\text{K}_2\text{Ti}_4\text{O}_9$ once again to form $\text{K}_2\text{Ti}_2\text{O}_5$. This mechanism is also supported by our previous studies, in which we have found a similar structure switching phenomenon between $\text{K}_2\text{Ti}_2\text{O}_5$ and $\text{K}_2\text{Ti}_6\text{O}_{13}$ induced by the gas phase sorption of molecular NO_x or

SO₂ at 500–600 °C.^{35, 36} With CO₂, the reason why K₂Ti₂O₅ changed into K₂Ti₄O₉, not K₂Ti₆O₁₃ is because the binding energy between K⁺ and carbonate ions is lower than that with nitrate/sulfate ions. Revealing the structural changes during CO₂ adsorption and desorption is not only important for understanding and designing of novel CO₂ adsorbents, but also crucial for practical application. For instance, some key operating parameters including theoretical CO₂ adsorption capacity, volume and heat changes during adsorption and desorption, and the highest temperature that can be applied, etc could be estimated from the structural changes mechanism.

The energy changes during CO₂ sorption on K₂Ti₂O₅ was calculated using density functional theory (DFT), as shown in Figure 8. The simulation results indicate that after losing two K atoms by adsorbing CO₂, if the resulting K₂Ti₄O₉* still remains its previous structure, the system energy will be increased by 13.8 eV, which makes the system being an unstable circumstance. However, the transformation of K₂Ti₄O₉* to K₂Ti₄O₉ can lead to the system energy being reduced by 50.6 eV and achieving a steadier state. Thus, from the theoretical prospective the DFT calculation further verified that feasibility of the proposed CO₂ sorption/desorption mechanism.

3.5 CO₂ sorption/desorption cycling test over K₂Ti₂O₅

For most of the high-temperature CO₂ adsorbents such as CaO, alkali zirconates, and alkali silicates, the cycling stability is crucial for their practical application. Although their CO₂ capture capacity may be quite high, how to effectively prevent sintering is a major issue in long term use. In this contribution, the long-term stability of K₂Ti₂O₅ during CO₂ sorption-desorption cycles was also evaluated. In order to figure out the

desorption conditions and explore the optimal desorption temperature of $\text{K}_2\text{Ti}_2\text{O}_5$, TPD of CO_2 was carried out. After adsorbing CO_2 at 750 °C, the sample was heated from room temperature to 800 °C with a heating rate of 5 °C/min. The desorbed CO_2 was monitored using an on-line quadrupole mass spectrometer. Figure 9 shows that CO_2 desorption begins at 600 °C, with a peak temperature of 714 °C. The CO_2 sorption-desorption cycling test of $\text{K}_2\text{Ti}_2\text{O}_5$ was evaluated using a typical pressure swing sorption (PSA) process. The sorption was performed with pure CO_2 at 750 °C for 60.0 min and the desorption was performed with pure N_2 at 750 °C for 10.0 min. Figure 9(b) shows the CO_2 sorption and desorption performance of $\text{K}_2\text{Ti}_2\text{O}_5$ during 20 cycles. There was no deterioration in the CO_2 uptake over 20 cycles. In contrast, the CO_2 uptake gradually increased within the first few cycles, and eventually became stable thereafter. As shown in Figure 9(b), the CO_2 uptake increased from 3.9 wt% in cycle 1 to 7.2 wt% in cycle 6. After cycle 6, there was almost no change in CO_2 sorption capacity and it maintained at *ca.* 7.2 wt%. Although the CO_2 capture capacity of $\text{K}_2\text{Ti}_2\text{O}_5$ is lower than that of CaO , $\text{K}_2\text{Ti}_2\text{O}_5$ exhibits superb stability during CO_2 sorption-desorption cycles, which is critical for its practical application.

To clarify why the CO_2 capture capacity actually increased with the increase in cycle numbers, the $\text{K}_2\text{Ti}_2\text{O}_5$ samples after cycle 1, cycle 6, and cycle 20 were analyzed using SEM. The XRD data in Figure 3 has demonstrated that after the desorption of CO_2 , the samples will transform back to $\text{K}_2\text{Ti}_2\text{O}_5$. Figure 10 shows the morphological change of $\text{K}_2\text{Ti}_2\text{O}_5$ after cycle 1, cycle 6, and cycle 20. Fresh $\text{K}_2\text{Ti}_2\text{O}_5$ showed big plate-like particles with clean and smooth surfaces (Figure 10(a)). While as increasing the cycle number from 1 to 20, the particles gradually cracked down and formed $\text{K}_2\text{Ti}_2\text{O}_5$

nanofibers (Figure 10(b–d)). Therefore, the improvement in CO₂ sorption capacity can be attributed to the morphological changes. Such formed K₂Ti₂O₅ nanofibers are more favorable for CO₂ sorption than the fresh K₂Ti₂O₅ whose particle size is much bigger.

4. Conclusion

In this contribution, in addition to the previous well studied Li₂ZrO₃ and Li₄SiO₄ as high-temperature CO₂ adsorbents, another type of alkali ceramic–potassium titanates, K₂Ti₂O₅ was investigated as a new type of high temperature CO₂ adsorbent for the first time. TGA analyses in CO₂ (carbonation process) demonstrated that only K₂Ti₂O₅ has the capability to capture CO₂, particularly at the temperature range 600–800 °C. Isothermal CO₂ sorption tests showed that the optimal sorption temperature for K₂Ti₂O₅ was 750 °C, with a capacity as high as 6.4 wt% after 2.0 h. By utilizing XRD, FTIR, SEM, TEM, and SAED analyses, the mechanism for the CO₂ sorption and desorption over K₂Ti₂O₅ was investigated, which can be explained by a reversible structure switching mechanism between K₂Ti₂O₅ and K₂Ti₄O₉, accompanied by the formation of K₂CO₃ species. The feasibility of the proposed CO₂ sorption/desorption mechanism was verified using DFT calculations. CO₂ sorption/desorption cycling tests proved that K₂Ti₂O₅ has excellent stability. In contrast to many adsorbents that deteriorate with cycles, the CO₂ uptake of K₂Ti₂O₅ gradually increased within the first few cycles, and eventually became stable afterwards (7.2 wt%). We also demonstrated that a rapid release of sorbed CO₂ can be achieved within only 6.0 min. The good CO₂ capture capacity, excellent cycling stability, and rapid regeneration indicates that K₂Ti₂O₅ would be a very promising high-temperature CO₂ adsorbent for the SEHP processes.

Acknowledgements

This work was supported by the Fundamental Research Funds for the Central Universities (2016ZCQ03), the National Natural Science Foundation of China (51572029, 51308045).

References

1. T. J. Crowley and R. A. Berner, *Science*, 2001, **292**, 870-872.
2. M. Meinshausen, N. Meinshausen, W. Hare, S. C. B. Raper, K. Frieler, R. Knutti, D. J. Frame and M. R. Allen, *Nature*, 2009, **458**, 1158-1163.
3. M. R. Raupach, G. Marland, P. Ciais, C. L. Quéré, J. G. Canadell, G. Klepper and C. B. Field, *Proc. Natl. Acad. Sci. U. S. A.*, 2007, **104**, 10288-10293.
4. D. M. D'Alessandro, B. Smit and J. R. Long, *Angewandte Chemie*, 2010, **49**, 6058-6082.
5. Q. Wang, J. Luo, Z. Zhong and A. Borgna, *Energy Environ. Sci.*, 2011, **4**, 42-55.
6. M. E. Boot-Handford, J. C. Abanades, E. J. Anthony, M. J. Blunt, S. Brandani, N. Mac Dowell, J. R. Fernández, M.-C. Ferrari, R. Gross, J. P. Hallett, R. S. Haszeldine, P. Heptonstall, A. Lyngfelt, Z. Makuch, E. Mangano, R. T. J. Porter, M. Pourkashanian, G. T. Rochelle, N. Shah, J. G. Yao and P. S. Fennell, *Energy Environ. Sci.*, 2014, **7**, 130-189.
7. L. Huang, J. Wang, Y. Gao, Y. Qiao, Q. Zheng, Z. Guo, Y. Zhao, D. O'Hare and Q. Wang, *J. Mater. Chem. A*, 2014, **2**, 18454-18462.
8. R. S. Haszeldine, *Science*, 2009, **325**, 1647-1652.

9. S. Xiang, Y. He, Z. Zhang, H. Wu, W. Zhou, R. Krishna and B. Chen, *Nature communications*, 2012, **3**, 954.
10. S. Chowdhury, G. K. Parshetti and R. Balasubramanian, *Chem. Eng. J.*, 2015, **263**, 374-384.
11. E. Andreoli, E. P. Dillon, L. Cullum, L. B. Alemany and A. R. Barron, *Sci. Rep.*, 2014, **4**, 7304.
12. D. P. Harrison, *Ind. Eng. Chem. Res.*, 2008, **47**, 6486-6501.
13. Z. Li, Y. Liu and N. Cai, *Int. J. Hydrogen Energy*, 2012, **37**, 11227-11236.
14. J. Wang, L. Huang, R. Yang, Z. Zhang, J. Wu, Y. Gao, Q. Wang, D. O'Hare and Z. Zhong, *Energy Environ. Sci.*, 2014, **7**, 3478-3518.
15. H. M. Jang, K. B. Lee, H. S. Caram and S. Sircar, *Chem. Eng. Sci.*, 2012, **73**, 431-438.
16. K. M. K. Yu, I. Curcic, J. Gabriel and S. C. Tsang, *ChemSusChem*, 2008, **1**, 893-899.
17. H. Pfeiffer, C. Vazquez, V. H. Lara and P. Bosch, *Chem. Mater.*, 2007, **19**, 922-926.
18. J. I. Ida and Y. S. Lin, *Environ. Sci. Technol.*, 2003, **37**, 1999-2004.
19. B. N. Nair, T. Yamaguchi, H. Kawamura and S. I. Nakao, *J. Am. Ceram. Soc.*, 2004, **87**, 68-74.
20. M. Kato, S. Yoshikawa and K. Nakagawa, *J. Mater. Sci. Lett.*, 2002, **21**, 485-487.
21. C. Gauer and W. Heschel, *J. Mater. Sci.*, 2006, **41**, 2405-2409.
22. K. Essaki, M. Kato and H. Uemoto, *J. Mater. Sci.*, 2005, **40**, 5017-5019.
23. G. Kresse and J. Hafner, *Phys. Rev. B*, 1994, **49** 14251-14269.

24. G. Kresse and J. Furthmüller, *Phys. Rev. B*, 1996, **54**, 11169-11186.
25. P. E. Blöchl, *Phys. Rev. B*, 1994, **50**, 17953-17979.
26. G. Kresse and D. Joubert, *Phys. Rev. B*, 1999, **59**, 1758-1775.
27. B. Hammer, L. B. Hansen and J. K. Nørskov, *Phys. Rev. B*, 1999, **59**, 7413-7421.
28. W. Hou, Q. Yan, B. Peng and X. Fu, *J. Mater. Chem.*, 1995, **5**, 109-114.
29. X. Lv, Z. Chen, Y. Wang, F. Huang and Z. Lin, *ACS applied materials & interfaces*, 2013, **5**, 11271-11275.
30. J. Ortiz-Landeros, C. Gómez-Yáñez and H. Pfeiffer, *J. Solid State Chem.*, 2011, **184**, 2257-2262.
31. D. Yamaki, T. Nakazawa, T. Tanifuji, T. Aruga, S. Jitsukawa and K. Hojou, *J. Nucl. Mater.*, 2004, **329-333**, 1279-1282.
32. E. Carella and M. T. Hernandez, *Ceram. Int.*, 2014, **40**, 9499-9508.
33. S. Andersson and A. D. Wadsley, *Nature*, 1960, **187**, 499-500.
34. Y. Cao, K. Zhu, Q. Wu, Q. Gu and J. Qiu, *Mater. Res. Bull.*, 2014, **57**, 162-169.
35. Q. Wang, J. H. Sohn and J. S. Chung, *Appl. Catal. B: Environ.*, 2009, **89**, 97-103.
36. Q. Wang and J. S. Chung, *Appl. Catal. A: Gen.*, 2009, **358**, 59-64.

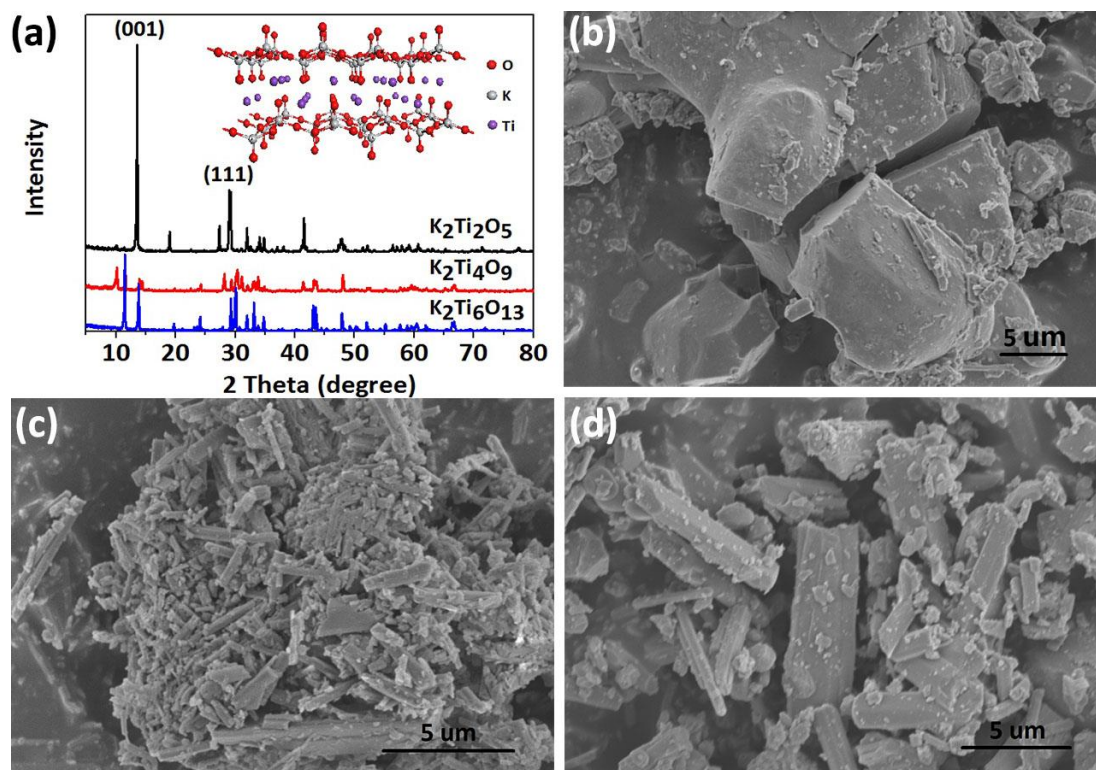


Figure 1. (a) XRD patterns of synthesized $K_2Ti_2O_5$, $K_2Ti_4O_9$, and $K_2Ti_6O_{13}$, and the inset shows the schematic structure of $K_2Ti_2O_5$, (b) SEM image of synthesized $K_2Ti_2O_5$, (c) SEM image of synthesized $K_2Ti_4O_9$, and (d) SEM image of synthesized $K_2Ti_6O_{13}$.

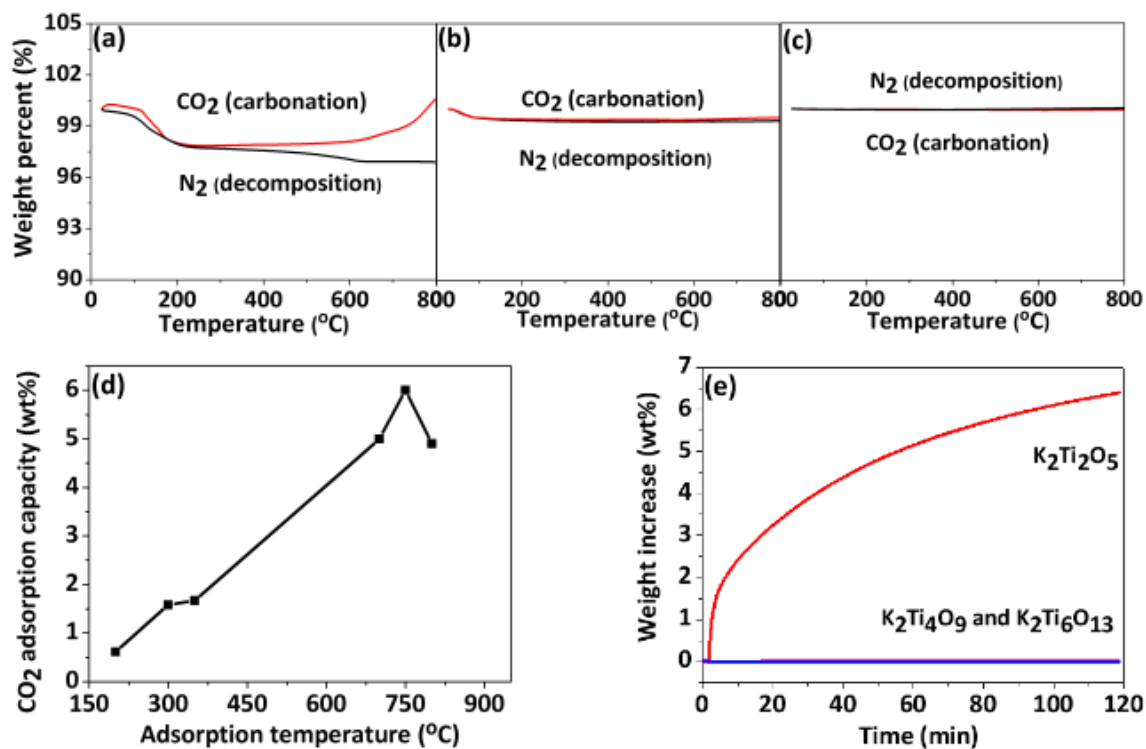


Figure 2. TGA analyses of (a) K₂Ti₂O₅, (b) K₂Ti₄O₉, (c) K₂Ti₆O₁₃ during decomposition (in N₂) and carbonation (in CO₂) processes, (d) The effect of sorption temperature on the CO₂ capture capacity of K₂Ti₂O₅, and (e) comparison of CO₂ capture capacity of K₂Ti₂O₅, K₂Ti₄O₉, and K₂Ti₆O₁₃ at 750 °C.

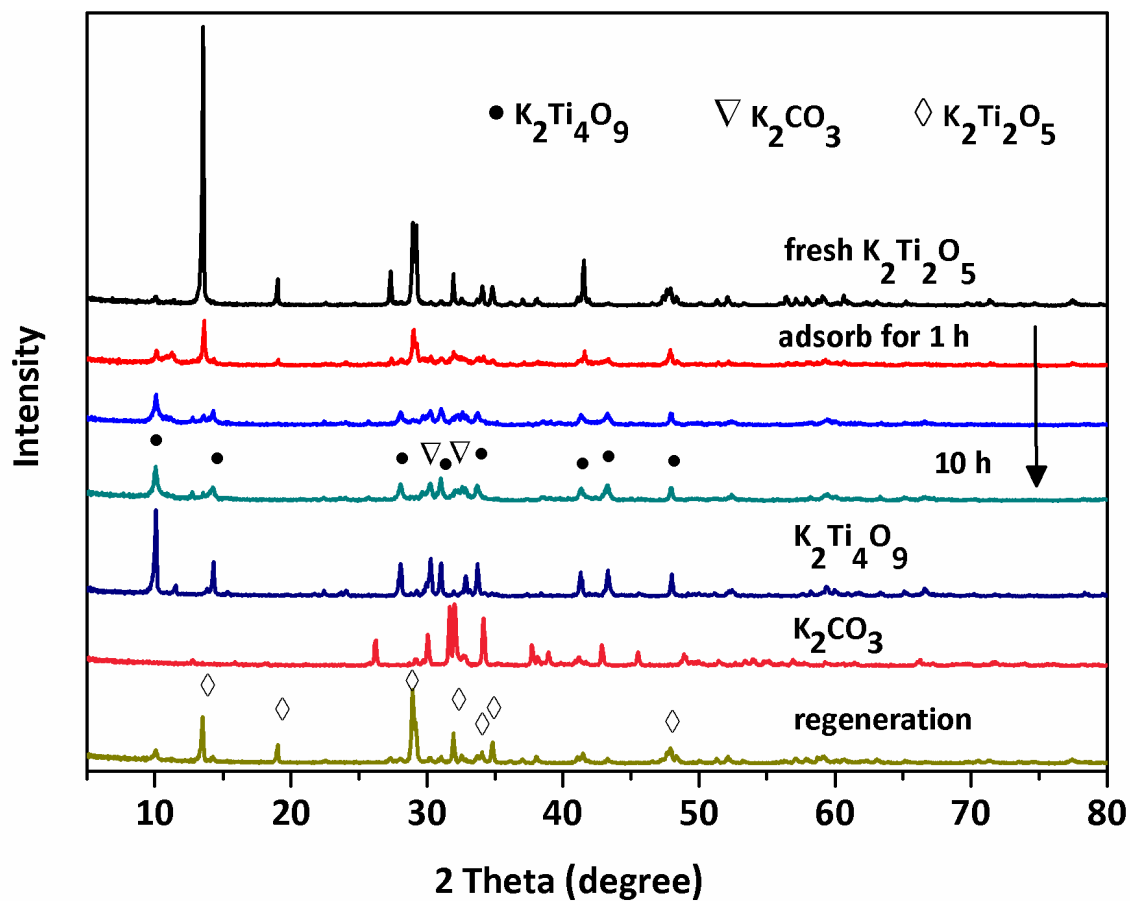


Figure 3. XRD patterns of fresh $K_2Ti_2O_5$, CO_2 -sorbed $K_2Ti_2O_5$ for 1.0, 5.0, and 10.0 h, fresh $K_2Ti_4O_9$, bulk K_2CO_3 , and regenerated $K_2Ti_2O_5$ sample.

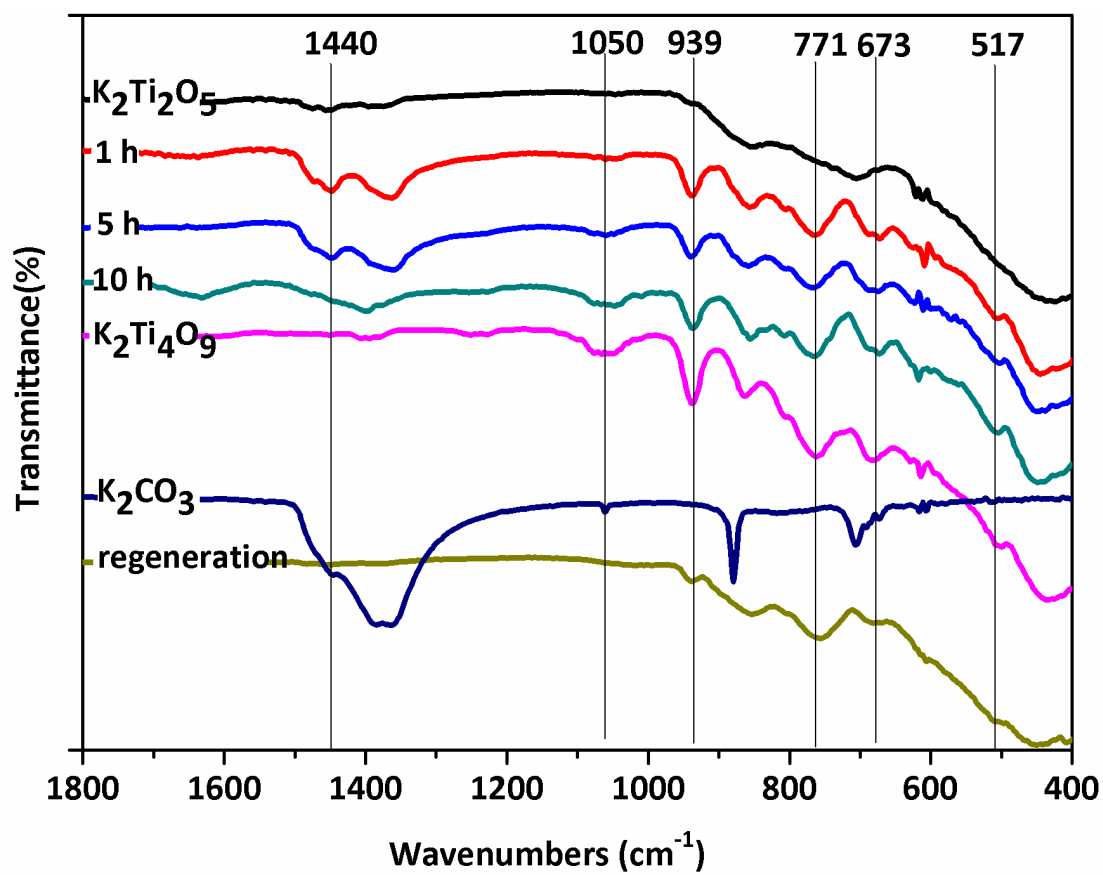


Figure 4. FTIR patterns of fresh $\text{K}_2\text{Ti}_2\text{O}_5$, CO_2 -sorbed $\text{K}_2\text{Ti}_2\text{O}_5$ for 1.0, 5.0, and 10.0 h, fresh $\text{K}_2\text{Ti}_4\text{O}_9$, bulk K_2CO_3 , and regenerated $\text{K}_2\text{Ti}_2\text{O}_5$ sample.

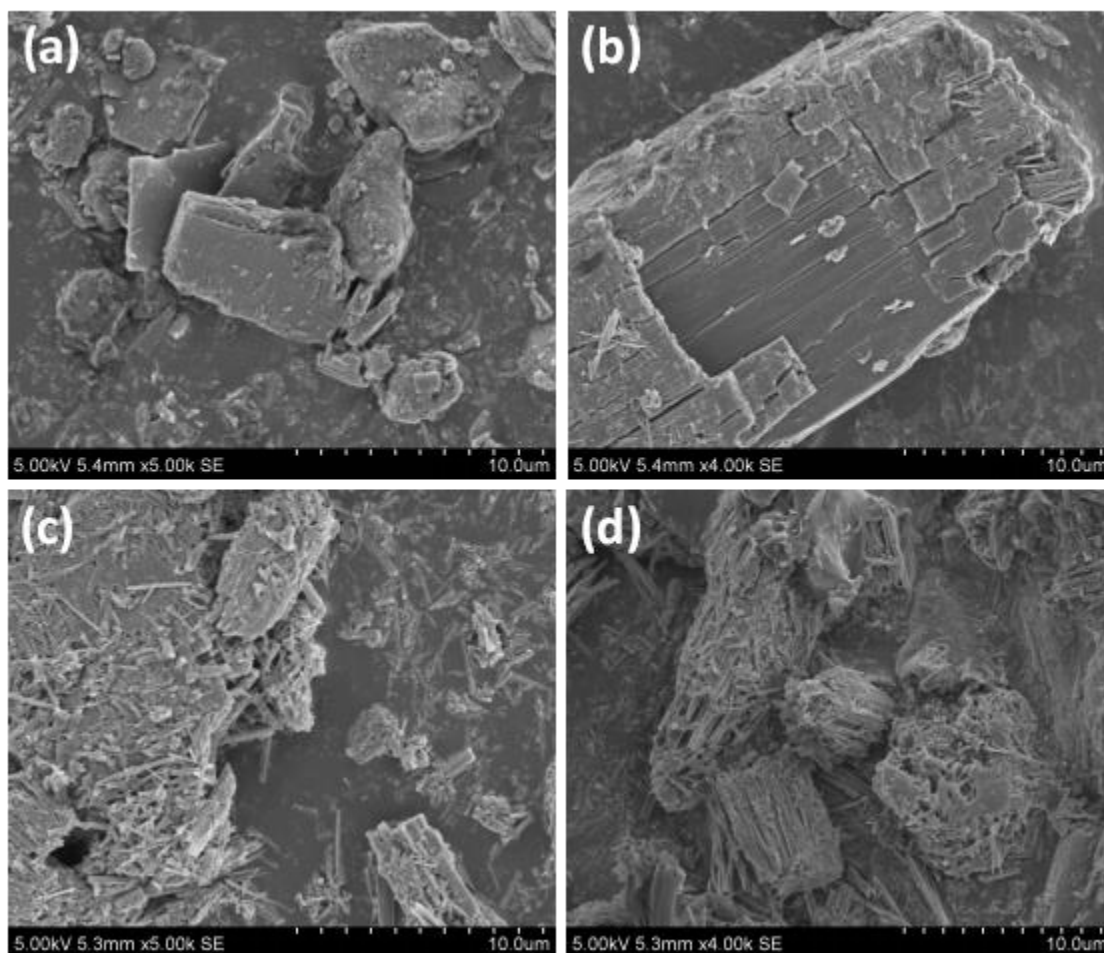


Figure 5. SEM image of (a) fresh $K_2Ti_2O_5$, (b) CO_2 -sorbed $K_2Ti_2O_5$ for 1.0 h, (c) CO_2 -sorbed $K_2Ti_2O_5$ for 5.0 h, and (d) CO_2 -sorbed $K_2Ti_2O_5$ for 10.0 h.

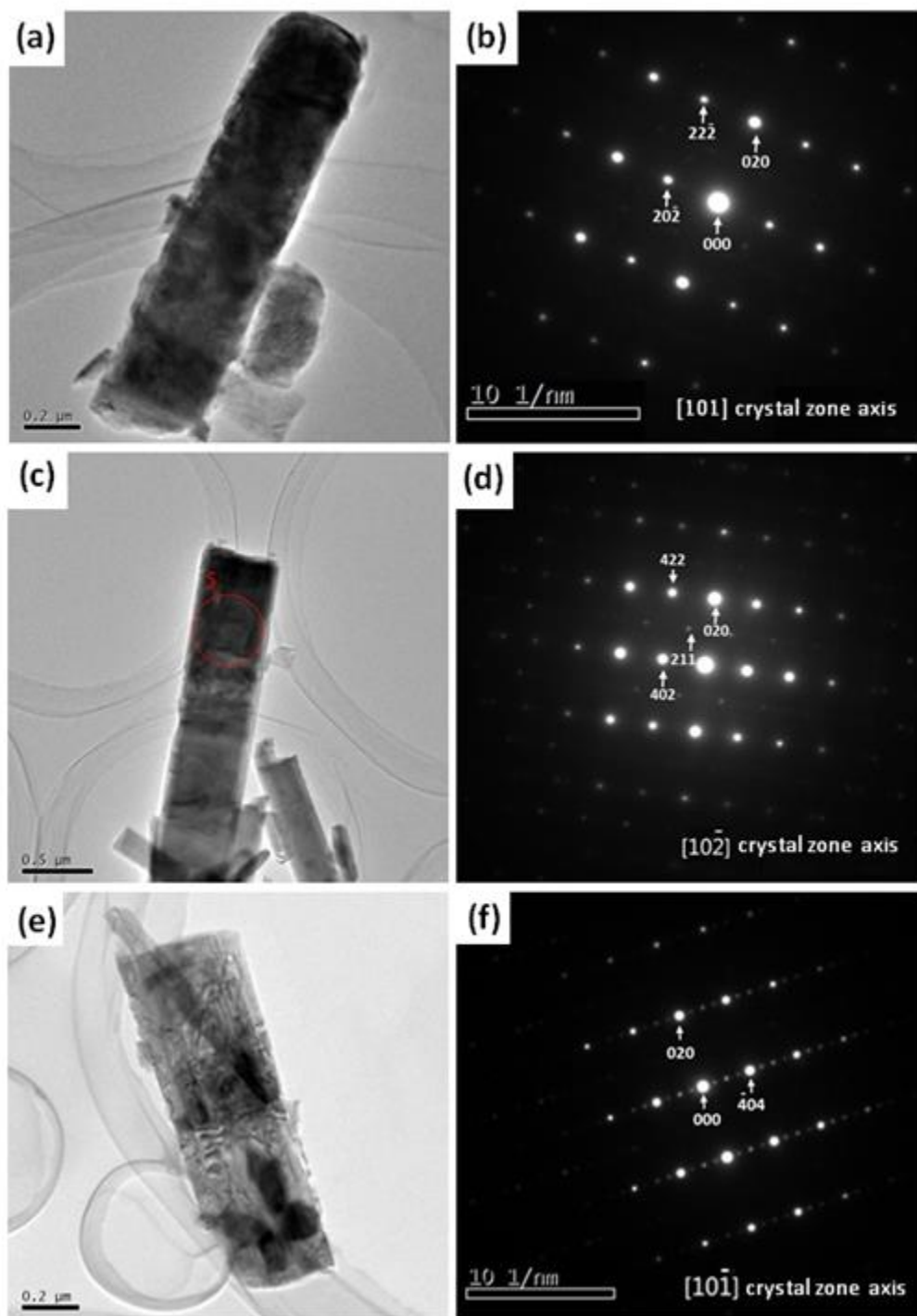


Figure 6. HR-TEM images of (a) fresh $\text{K}_2\text{Ti}_2\text{O}_5$, (c) fresh $\text{K}_2\text{Ti}_4\text{O}_9$, and (e) CO_2 -sorbed $\text{K}_2\text{Ti}_2\text{O}_5$ for 10.0 h, and SAED patterns of (b) fresh $\text{K}_2\text{Ti}_2\text{O}_5$, (d) fresh $\text{K}_2\text{Ti}_4\text{O}_9$, and (f) CO_2 -sorbed $\text{K}_2\text{Ti}_2\text{O}_5$ for 10.0 h.

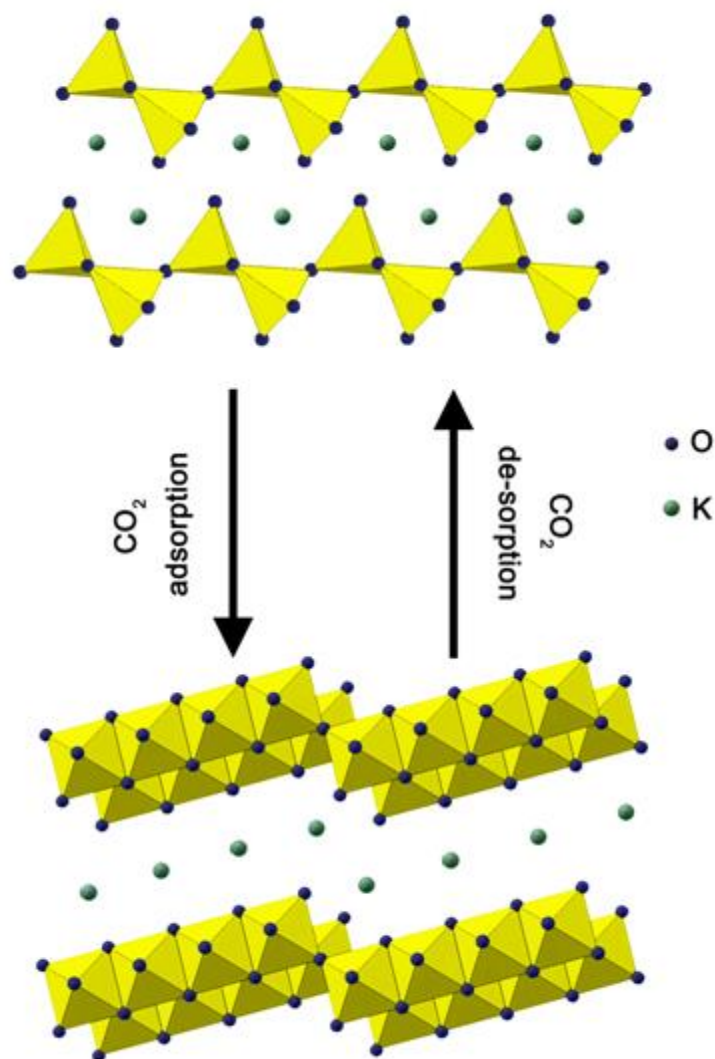


Figure 7. The proposed mechanism of $\text{K}_2\text{Ti}_2\text{O}_5$ – $\text{K}_2\text{Ti}_4\text{O}_9$ structure switching caused by CO_2 sorption and desorption.

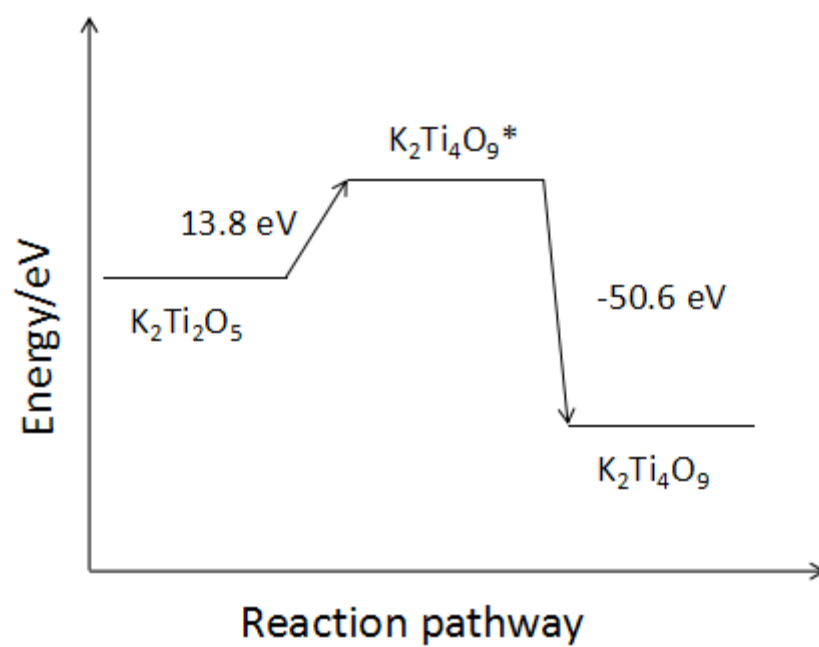


Figure 8. The energy change of CO₂ capture process calculated using DFT method, $K_2Ti_4O_9^*$ means the intermediate state of $K_2Ti_2O_5$ after the sorption of CO₂.

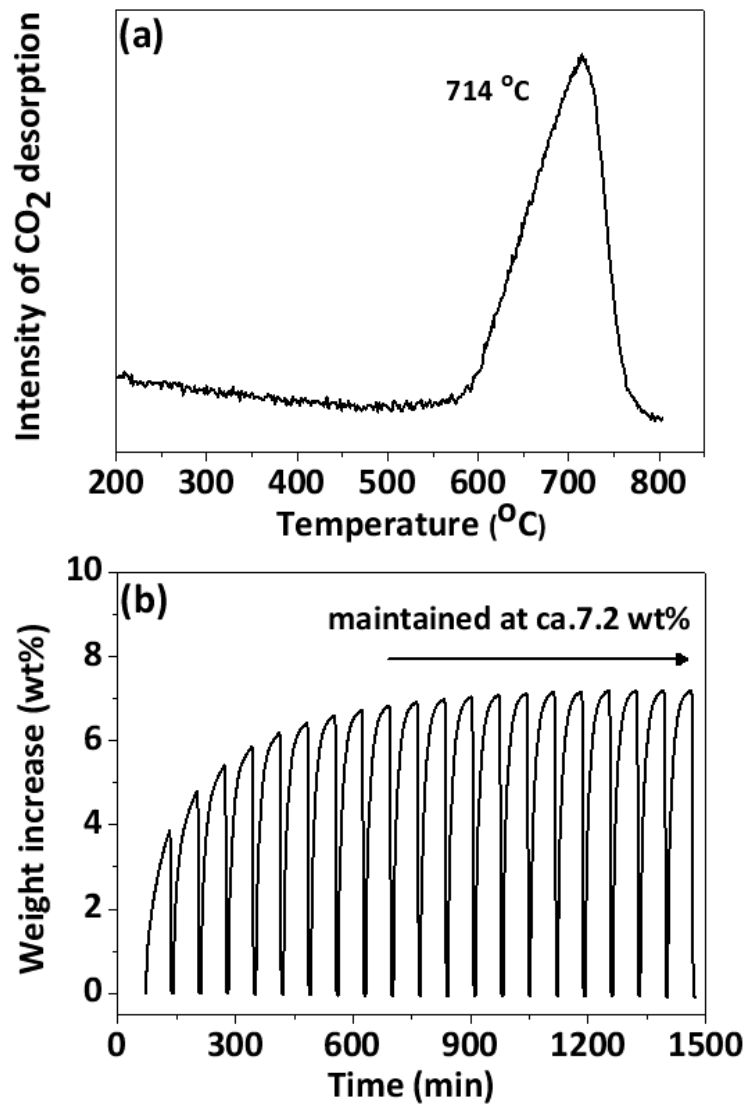


Figure 9. (a) TPD analysis of CO₂-sorbed K₂Ti₂O₅, and (b) CO₂ sorption-desorption cycling test over K₂Ti₂O₅.

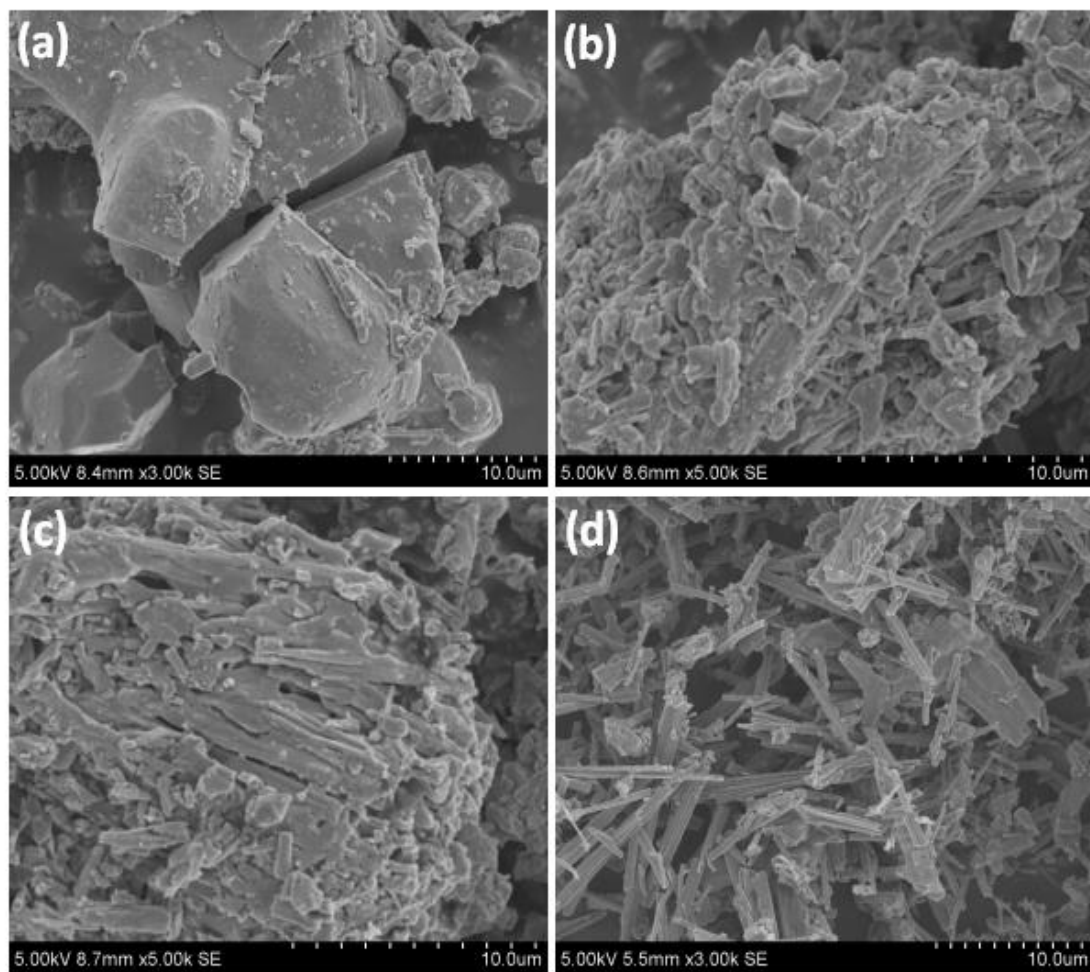


Figure 10. SEM images of (a) fresh $K_2Ti_2O_5$, and $K_2Ti_2O_5$ after (b) cycle 1, (c) cycle 6, and (d) cycle 20.